Image Cover Sheet

CLASSIFICATION	SYSTEM NUMBER
UNCLASSIFIED	141646

TITLE

CONSTANT AMPLITUDE FATIGUE CRACK GROWTH IN ALUMINUM-LITHIUM

AN: 94-03043

System Number:

Patron Number:

Requester:

Notes:

DSIS Use only:

Deliver to: BA

14.

"Constant Amplitude Fatigue Crack Growth in Aluminum-Lithium"

Z. Zhai and J. Morrison

DREP.Victoria, B.C.

Constant Amplitude Fatigue Crack Growth in Aluminum-Lithium

Zhen Hua Zhai and Jack Morrison

Defence Research Establishment Paciific
Victoria, B.C.

INTRODUCTION

A number of studies (1-5) of the constant load amplitude fatigue crack growth behaviour of aluminum-lithium alloys have indicated an improvement over conventional alloys. Important contributions to the reduction in crack extension rates include roughness induced crack closure, deviations from the intended crack plane, and non-planar propagation of the crack. All of these effects reduce the effective stress intensity at the crack tip. The anisotropy of mechanical properties and the strong texture found in these alloys, which has been argued to promote inhomogenous plastic deformation and planar slip also results in a variability of crack growth behaviour with the orientation of the fracture plane (6-7).

This paper describes a detailed study of the orientation dependence of fatigue crack growth in aluminum-lithium plate compared to conventional aerospace alloys. The materials studied were the same 8090, 2090, 2024, and 7075 plates described in the previous paper (8). Likewise the same six compact specimen orientations were employed for the aluminum-lithium tests (fig. 1), plus the L-T and T-L orientations for the 2024 and 7075 specimens.

EXPERIMENTAL PROCEDURES

The constant amplitude fatigue crack propagation tests were conducted in accordance with ASTM Standard E647 using 50 mm wide full plate thickness compact specimens. There is a marked tendency of fatigue cracks in the aluminum-lithium alloys to deviate from the intended crack plane. It was decided that, for the purposes of this study, the crack growth rates would be measured as far as possible solely in the direction of interest. Therefore, in order to keep the fatigue cracks extending normal to the applied load, the specimens were sidegrooved 10% of thickness on each side. In this way it was hoped that a well defined stress intensity and stress ratio could be maintained. Given the known directionality of properties in the aluminum-lithium alloys (9), it was recognized that this procedure might not reflect the behaviour of cracks in real structures. The alternative procedure would be to allow the fatigue cracking to proceed in whatever direction it deviated towards, and modify the stress intensity accordingly to account for the out of plane loading.

The tests were carried out under ambient conditions (about 35% relative humidity) in a servohydraulic testing machine controlled by a 386 model computer running the Instron program, "Advanced Fatigue Crack Propagation". Crack length was monitored automatically using unloading compliance determined from a clip gauge placed on the specimen load line. The initial notch length was approximately 12 mm. Very little load shedding was employed, precracking being carried out at a load close to the start ΔK for the test, which resulted in an initial crack extension rate of about 10^{-5} mm/cycle. The tests were conducted using a triangular waveform at a frequency of 10 Hz, and at two load ratios (R = 0.1 and 0.5). Data were collected at crack length increments of 0.6 mm. On completion of the test, an optical examination was made of the fractured specimen. Crack growth rates were calculated using unsmoothed point-to-point averaging. A detailed fractographic study of these specimens using scanning electron microscopy is described in the following paper (10).

RESULTS AND ANALYSIS

a) 2024-T351 and 7075-T651

Figures 2 and 3 show da/dN versus ΔK curves for the 2024-T351 and 7075-T651 specimens from the two orientations at each of the two R ratios. It can be seen that, as has often been observed (11), the stiffer 7075 alloy generally has a higher crack growth rate at a given ΔK. Likewise the end of the threshold and onset of power law crack growth occurs at a higher da/dN in the 7000 series alloy, indicative of the stronger influence of closure in this alloy. There is only a small orientation dependence in T-L and L-T. Increasing the R ratio results in a small increase in the separation of the 7075 and 2024 curves at low and intermediate ΔK. In the linear Stage II region of these curves, the slope is approximately 3 for alloy 7075, and about 3.5 for 2024 alloy.

In figs. 4 and 5 the above data are replotted to show more clearly the retardation of crack growth rates at low stress ratios. The difference found in the threshold region decreases approaching the linear stage 2, but there is still a persistent separation thereafter. The irregular crack growth rates at low stress intensity levels are largely eliminated by increasing the stress ratio.

A small but systematic trend with orientation was observed (fig. 6) by plotting the number of cycles as a function of the stress intensity range, starting at the same load and crack length at an arbitrary zero cycles. This effect may be related to the lower fracture toughness in the T-L orientations, and seems reproducible, although there were not many suitable specimens for comparison with the same initial crack lengths and ΔK values, the final precracking being carried out so as to give a desired crack growth rate. Interestingly enough, increasing the load ratio appears to decrease the apparent orientation effect, pointing to an orientation dependent closure as one contributor.

In both the 2024-T351 and 7075-T651 specimens, the fatigue cracks grew across the specimen within the side grooves and normal to the applied load without significant deviation. The fatigue cracks were smooth (fig. 7).

b) 8090-T877

Figures 8 and 9 show da/dN versus ΔK curves for the 8090-T8771 specimens from the six orientations at each of the two R ratios. A pronounced orientation dependence is observed, both in crack growth rate and fracture appearance.

In the L-T and T-L orientations, the fatigue fracture surfaces observed on the 8090 alloy specimens are much rougher than in 2024-T351 and 7075-T651 (figure 10a). In the remaining 8090 orientations (fig. 11), the cracks start off smooth (fig. 10b), but increasingly roughen from the edges inwards as the crack extends. This may be the result of the fact that ΔK is increasing as the crack grows. It is assumed that the dark rough surfaces result from fretting as a result of crack closure. Only in the L-T orientation did the crack remain perpendicular to the applied loading direction, otherwise the cracks grew out of the intended fracture plane despite the constraint provided by the side-grooves. There is, however, a restraining effect of the side grooves near the surface. For example, in the L+30 orientation viewed end-on in the crack growth direction, the fatigue fracture surface bulges up in a thumbnail shape across the specimen thickness. In the T-L orientation, the crack grew markedly away from the intended plane. At R = 0.1, it deviated at an angle of about 52° at a very early stage of growth, and remained at that angle until unstable rupture occurred (fig. 10b), whereas at R = 0.5, the crack only deviated in this manner after zig-zagging several times, leaving behind a laminated, saw-toothed surface (figure 10c).

In figure 11, the 8090 specimens are arranged with the same surface of the plate uppermost. The deviation of the crack from its intended plane is not random. In the L+30 and

L+150 orientations (with the intended crack plane at 60° either side of the rolling direction) , the cracks tilted about 5° towards the rolling direction, changing the crack growth planes to ±55° from the rolling direction, which has been reported to be the softest tensile orientation. This is obviously the same orientation towards which the T-L samples deviated. It has also been determined elsewhere (12) that the texture in the centre of 8090 plate is {110}<112>, so that the ±55° directions correspond to [110] slip directions. For the most part these specimens had smooth fracture appearances.

In the L+60 and L+120 orientations (crack growth nominally at ±30° to the rolling direction), the cracks deviated about five degrees away rather than towards the rolling direction, growing for most of the test at ±65° to the rolling direction. As part of this process there was also a tendency for the crack to step completely out of the intended plane. This may reflect the fact that although the crack would prefer to grow at the larger angle, once it has left the groove the relaxed constraint prevents it from doing so. At a high stress intensity near the end of the test, the cracks further deviated towards the ±55° orientations. These specimens initially generated smooth fracture surfaces, but as the cracks deviated and the cyclic stress intensity increased, the smooth region was gradually squeezed into a triangle at the specimen centre. This suggests that a change in fatigue mechanism occurs above some minimum ΔK.

Given the normal scatter expected in the da/dN vs. ΔK plots, with the exception of the T-L specimens, there is little orientation dependence indicated in figs. 8 and 9, and the overall trends are similar. The T-L curves show the strong effect of the large deviation in fracture plane on crack growth retardation, but the smaller deviations described above for the other orientations tend to result in similar curves, which cannot be ranked systematically. Not surprisingly there is a strong stress ratio effect on the shape of these curves, with the higher R ratio reducing the observed closure effect (figure 12). The crack growth rates at R=0.5 are markedly higher than at R=0.1, and the effect is stronger than in the conventional alloys. The stress ratio effect is also less marked in the T-L compared to the other orientations. It is interesting to note that the low propagation rate T-L orientation also has the lowest measured fracture toughness.

c) 2090-T8E41

Figures 13 and 14 show da/dN versus ΔK curves for the 2090-T8E41 specimens from the six orientations at each of the two R ratios.

It has been reported (11) that in the centre of 2090-T8E41 plate, the texture is the same as that found in the 8090-T8771 plate, namely {110}<112>, but is much less intense near the surface. This may be why the fracture surfaces of 2090-T8E41 specimens differ from those of 8090-T8771 (figures 15 and 16). In 8090-T8771, the crack in T-L orientation grew out of the original plane across virtually the entire thickness, whereas in 2090-T8E41 the deviation occurs mainly in the centre, and the deviation is not as severe (figure 15a). During most of the growth, the crack centre meandered along a path inclined at less than 45 degrees from the intended fracture plane. Only at a very late stage did the crack approach 55° from the rolling direction. In 8090 the L-T orientated crack managed to stay on the intended plane, but in 2090, at R = 0.1, the L-T fracture surface also grew out of plane, although not as far as in the T-L orientation. The general appearance of cracks growing in the remaining 4 orientations is similar in 2090 to 8090. However, in contrast to 8090, the fracture surfaces of the L+30 and L+150 alloy 2090 specimens are rough (fig. 15b), and again the edges have a strong tendency to stay within the side grooves. In 2090 specimens the fracture surfaces in the L+60 and L+120 orientations are the smoothest. The overall appearances are shown in Figure 16.

The variations in texture may also explain the apparent increase in da/dN darta scatter in 2090 alloy seen in figs. 13 and 14 (excluding L-T and T-L). Other than in the L-T and T-L

specimens, the trends are similar to those in 8090. In 2090 there is an indication that, at growth rates below 10^{-4} mm/cycle, the L+60 and L+120 specimens show higher gowth rates at a given ΔK. This trend is not apparant in the 8090 results. The dependence of crack growth rate on stress ratio in 2090 seems somewhat smaller than in the 2024, 7075 and 8090 (figure 17).

Figures 18 and 19 show crack growth data from the orientations with the fastest crack growth rates for each alloy respectively at each stress ratio. The lithium containing alloys have similar crack growth rates, and their strong stress ratio effect compared to the conventional alloys is apparent. 2090 (and 8090 at R=0.5) appears to undergo faster crack growth than 2024 at low ΔK, otherwise the aluminum-lithium alloys are more fatigue crack groowth resistant than the 2024 or 7075 alloys.

A more detailed analysis of data repeatability at the different orientations would be needed to conclusively evaluate the orientation effects. Likewise there is a need to evaluate the crack growth behaviour in specific directions, notably at $\pm 35^{\circ}$ and $\pm 55^{\circ}$ to the rolling direction. The orientation and R ratio effects indicated in the above data are also being subjected to a crack closure analysis based on ΔK_{eff}.

CONCLUSIONS

1. In 2024-T351 and 7075-T651 plates, the T-L orientation yields faster crack growth rates than L-T. An increasing R ratio reduces this effect.

2. Fatigue crack propagation in 2090-T8E41 and 8090-T8771 plates is orientation dependent. The T-L orientation is the most resistant.

3. Strong closure effects are seen in aluminum-lithium alloys. The R ratio has no effect on orientation dependence in 2090 and 8090 alloys, but markedly affects the rate of crack propagation.

4. 2090 and 8090 both show superior resistance to crack propagation to 7075-T651 plate even in the weakest orientations. At low stress intensity ranges and high stress ratios, aluminum - lithium is slightly less resistant than alloy 2024.

REFERENCES

1. R.J.H. Wanhill, "Status and Prospects for Aluminium-Lithium Alloys in Aircraft Structures", *Fatigue of Metallic Materials*, Elsevier, 1992, pp. 43-82.

2. Venkateswara Rao, K.T., Yu W., and Ritchie, R.O., "Fatigue Crack Propagation in Aluminum-Lithium Alloy 2090: Part I. Long Crack Behaviour", Metallurgical Transactions A, **19A**, (1988), pp. 549-561.

3. Peters, M., Welpmann, K., McDairmaid, D.S., 't Hart, W.G.J., "Fatigue Properties of Al-Li Alloys", *New Light Alloys*, Proceedings No. 44, Advisory Group for Aerospace Research and Development, (1089), pp. 6-1 - 6-18.

4. Venkateswara Rao, K.T., Bucci, R.J., Jata, K.V., and Ritchie, R.O., "A Comparison of Fatigue Crack Propagation Behaviour in Sheet and Plate Aluminum-Lithium Alloys, Materials Sci. and Engineering, **A141**, (1991), pp. 39-48.

5. Peters, M., Welpmann, K., Zink, W., and Sanders, T.H. Jr., "Fatigue Behaviour of Al-Li-Cu - Mg Alloys,*Aluminuum Alloys III*, The Institute of Metals, (1986), pp. 239-246.

6. Bréchet, T., and Louchet, F., "Fatigue of Al-Li Alloys: Mechanical Properties, Microstructure (TEM and SEM) and Strain Localization", J. Materials Sci., **25** (1990), pp. 3053-3060.

7. Jata, K.V., and Starke, E.A. Jr., "Fatigue Crack Growth and Fracture Toughness Behaviour of an Al-Li-Cu Alloy", Metallurgical Transactions A, **17A,** (1986), pp. 1011-1026.

8. Morrison, J., Zhai, Z., and KarisAllen K.J., "Directionality of Strength and Toughness In ALuminum-Lithium Plate", Proc. Workshop *Research and Development on Aluminum-Lithium Alloys, (efence Research Establishment Pacific, (1993),* pp. 287-304.

9. N. Eswara Prasad and G. Malakondaiah, "Anisotropy of Mechanical Properties in Quaternary Al-Li-Cu–Mg Alloys", Bull. Mater. Sci., **15,** No. 4, (1992), pp. 297-310.

10. Hull, D.A., "A Fractographic Study of Selected Aluminum-Lithium Alloys", Proc. Workshop *Research and Development on Aluminum-Lithium Alloys, (efence Research Establishment Pacific, (1993),* pp.?????,.

11. Paris, P.C., "Twenty Years of Reflection on Questions involving Fatigue Crack Growth, Part I: Historical Observations and Perspectives", *Fatigue Thresholds Vol. 1*, EMAS Publications, (1981), pp. 3-10.

12. Squibb, M.W., and Wilson, R.N., "The Fatigue and Fracture Behaviour of Aluminum - Lithium Plate - UK Study", Proc. Workshop *Research and Development on Aluminum-Lithium Alloys, Defence Research Establishment Pacific, (1993),* pp.215-240.

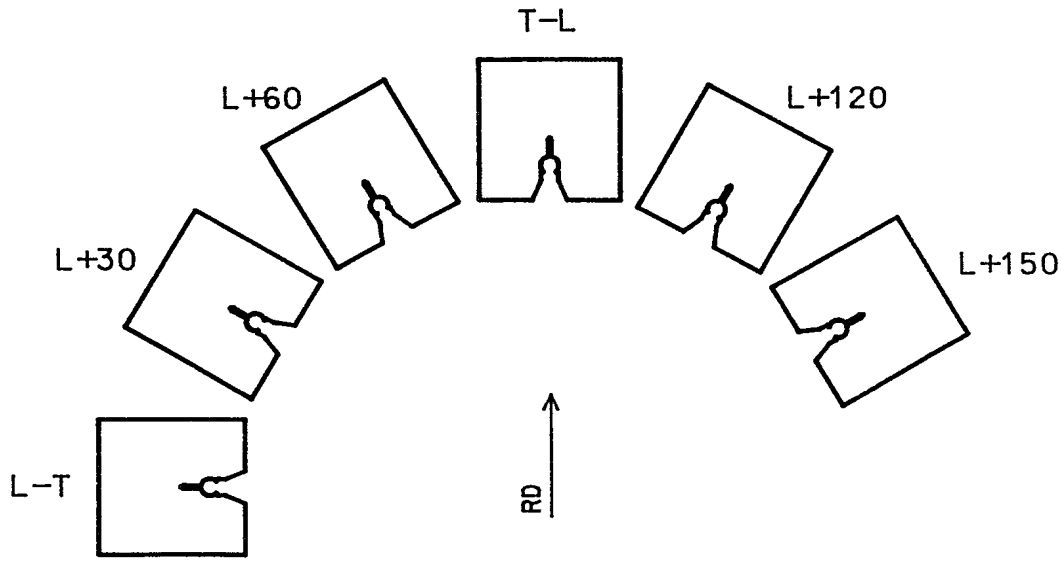

Figure 1. Aluminum-lithium specimen orientations.

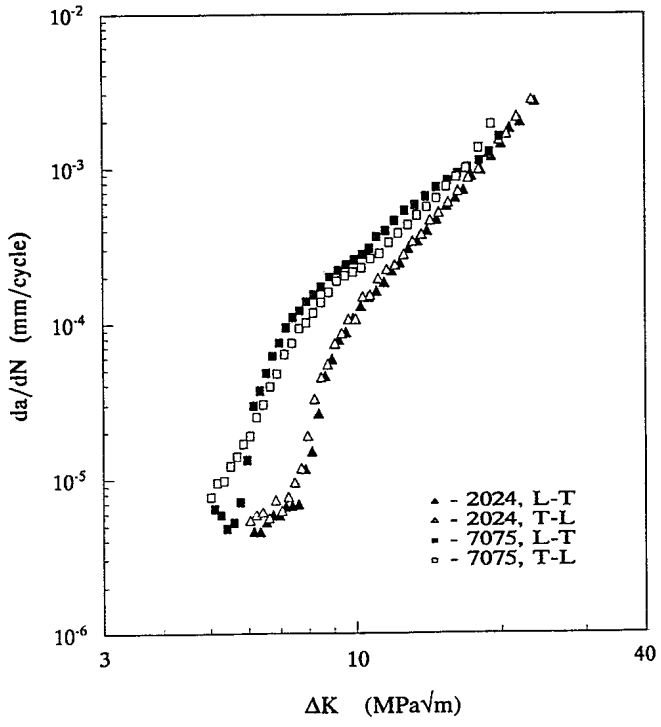

Figure 2. Fatigue crack growth rate versus stress intensity factor range for 2024-T351 and 7075-T651 plates. R = 0.1.

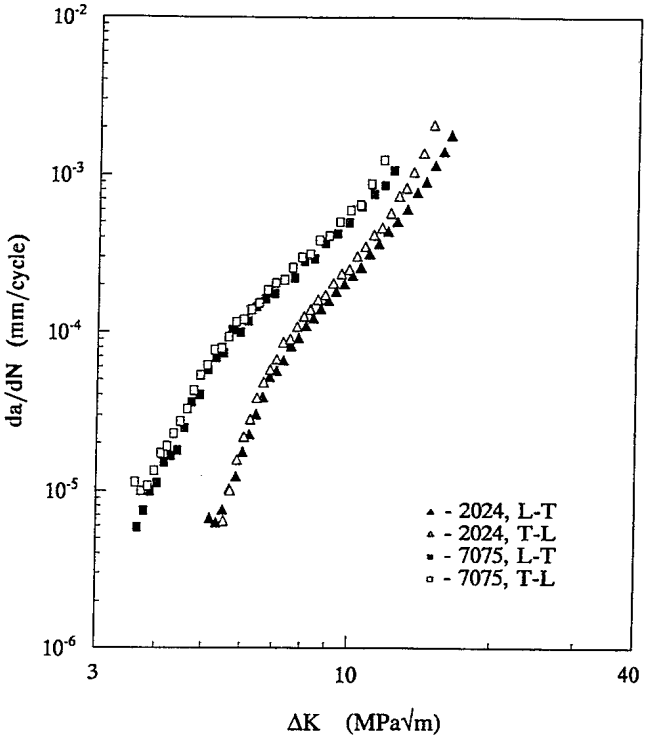

Figure 3. Crack growth rate versus stress intensity range for 2024 and 7075 at R = 0.5.

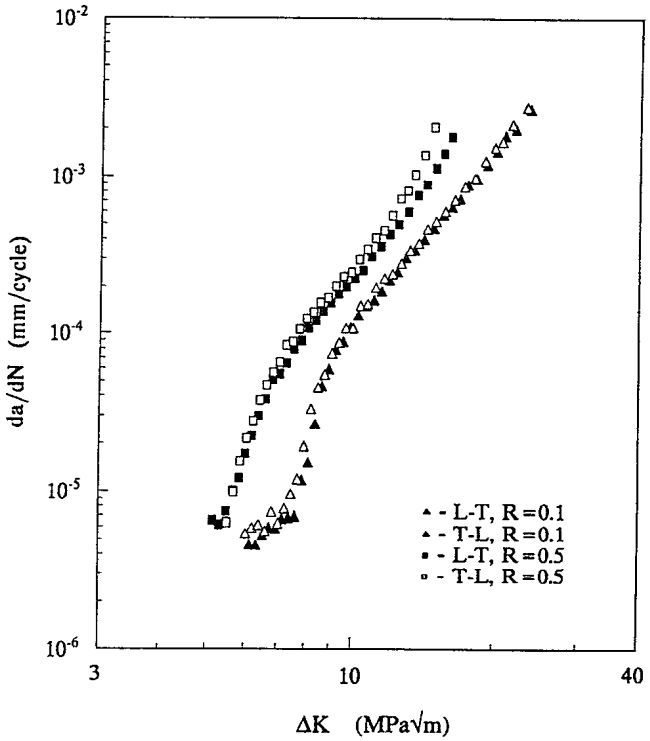

Figure 4. The effect of R ratio on crack growth in 2024.

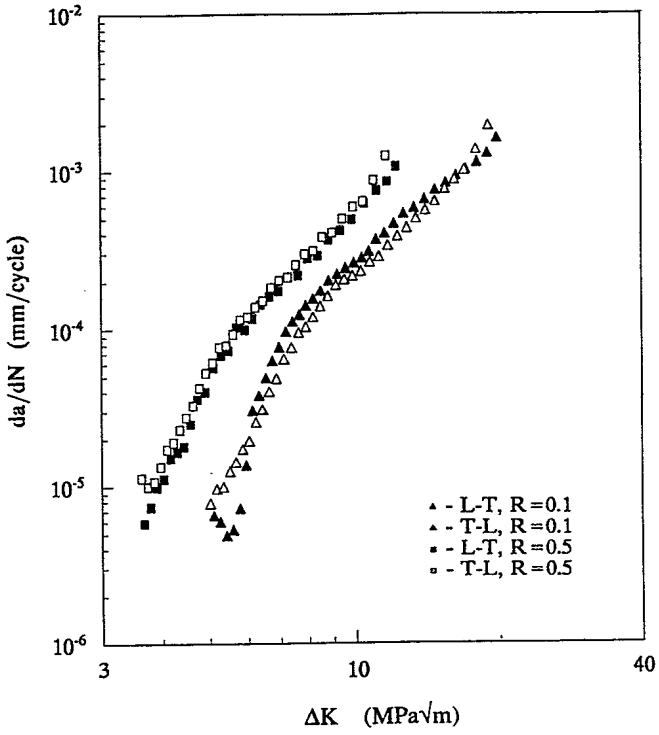

Figure 5. The effect of R ratio on crack growth in 7075.

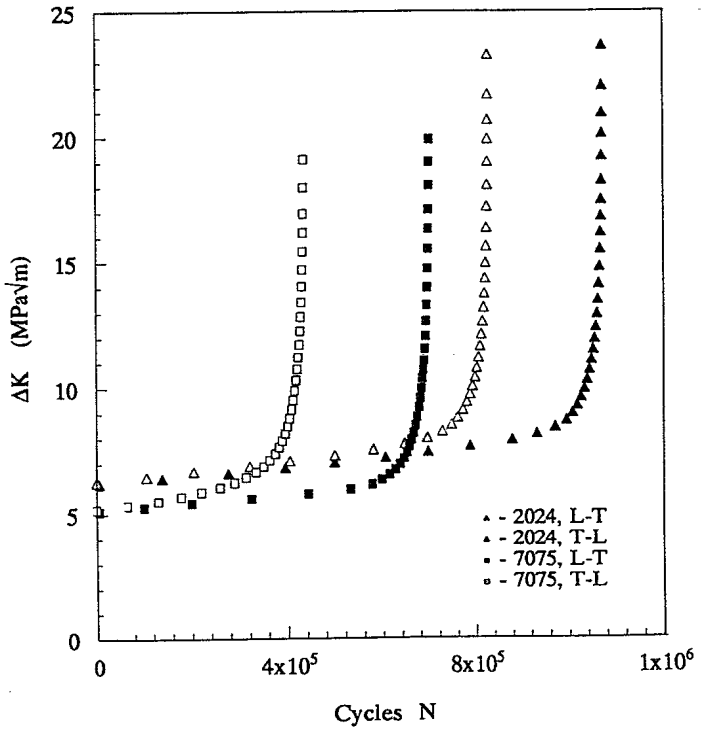

Figure 6. Crack length in ΔK as a function of elapsed cycles in 2024 and 7075 at R = 0.1. Initial crack length nominally 15 mms.

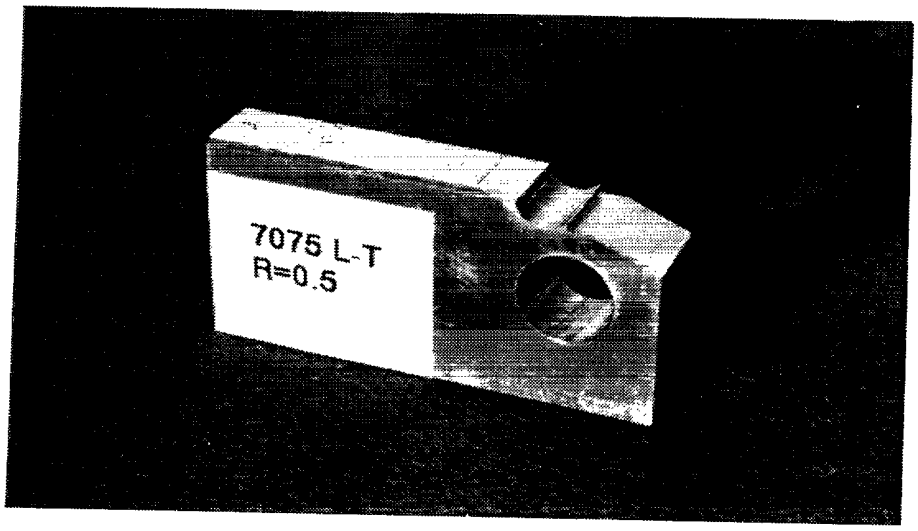

Figure 7. Fracture surface in the L-T orientation in 7075.

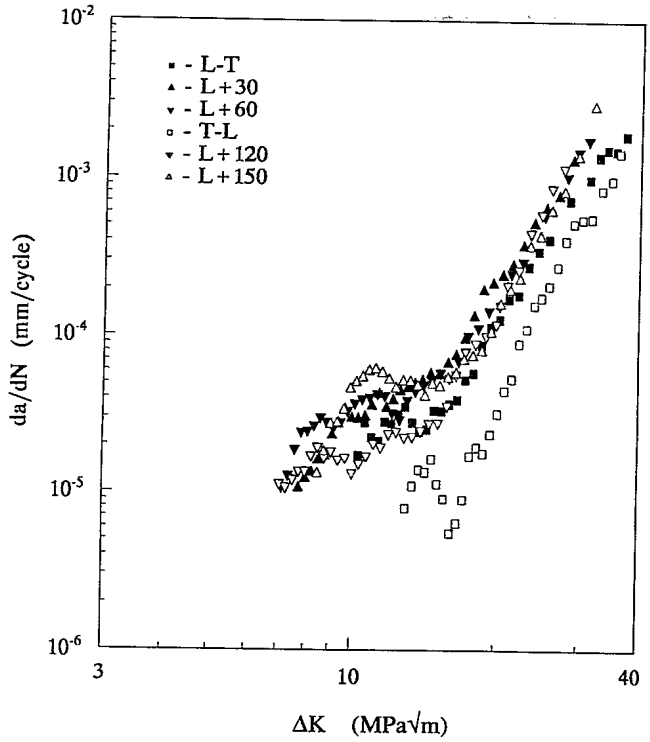

Figure 8. Fatigue crack growth rate versus stress intensity factor range for 8090-T8771 plate at R = 0.1.

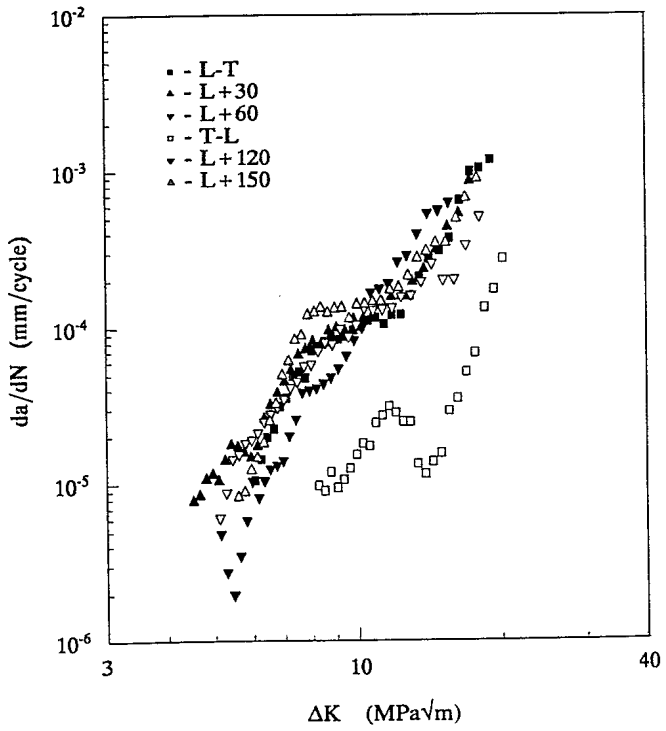

Figure 9. Crack growth rate versus stress intensity factor range for 8090 at R = 0.5.

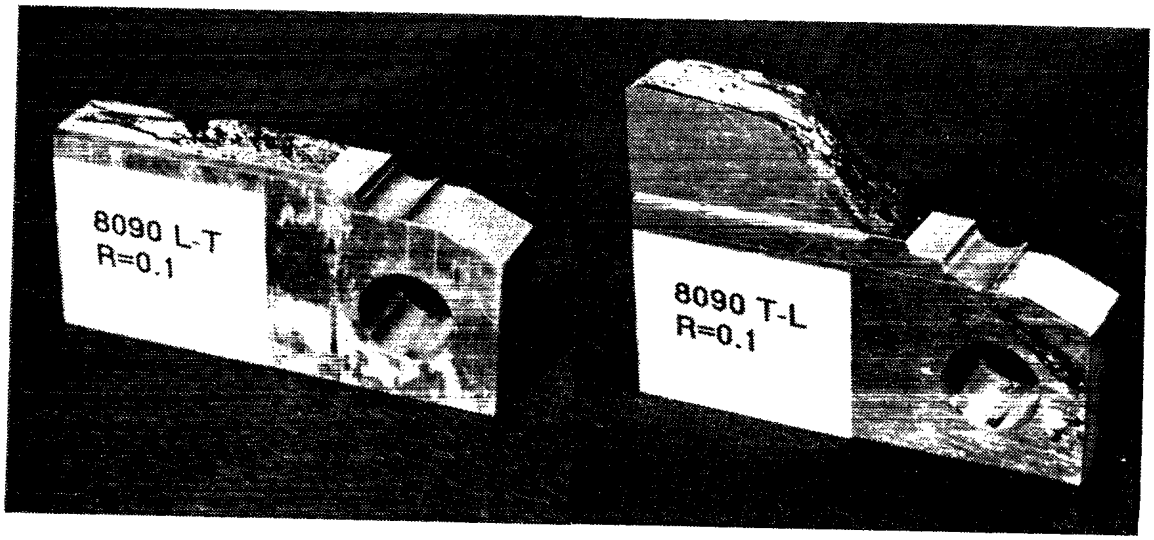

(a) (b)

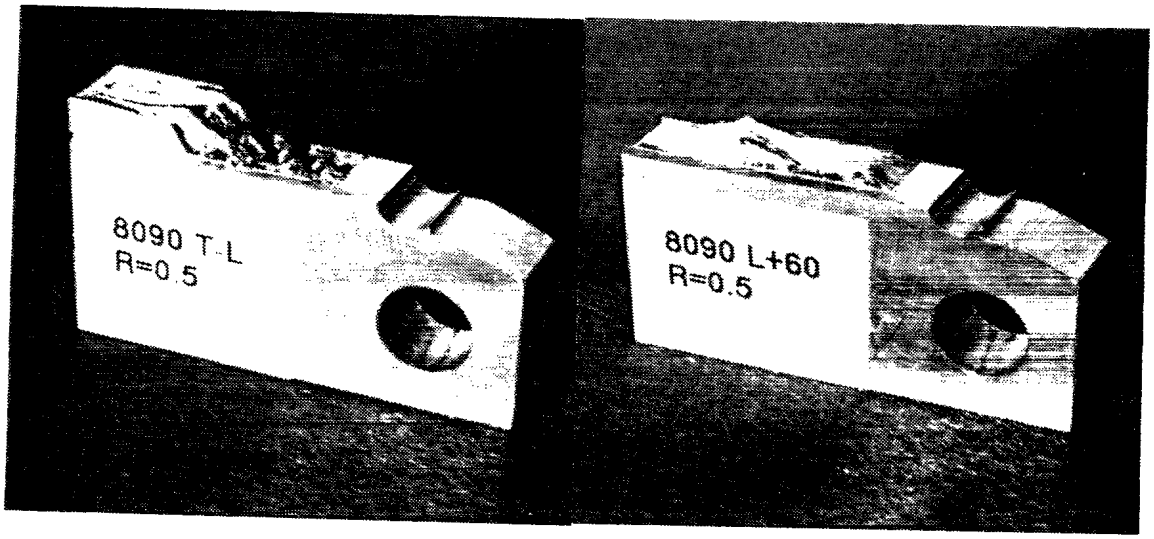

(c) (d)

Figure 10. Fracture surfaces of 8090 plate.

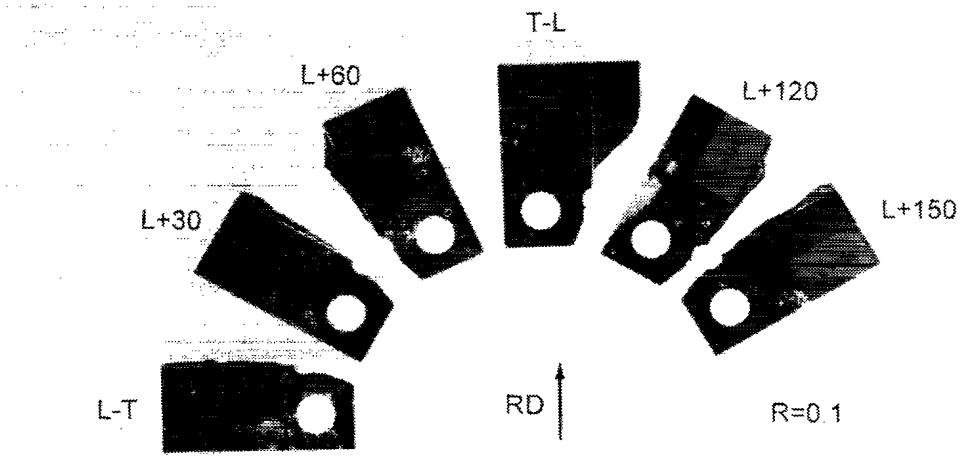

(a)

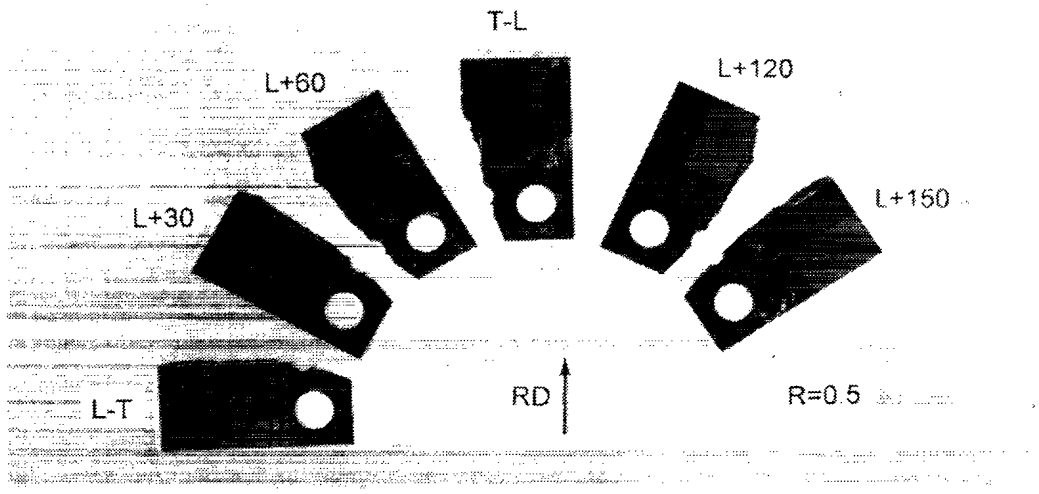

(b)

Figure 11. Profiles of broken 8090 specimens.

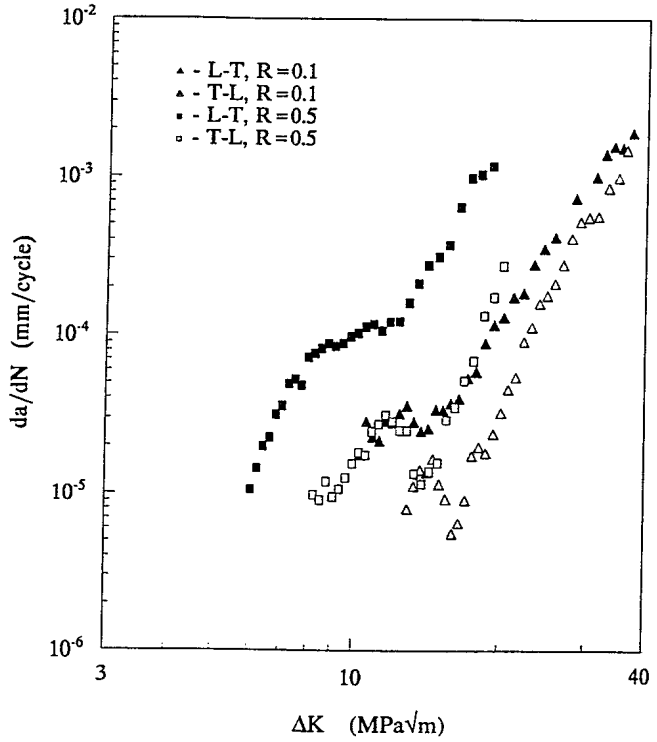

Figure 12. The effect of R ratio on crack growth in 8090.

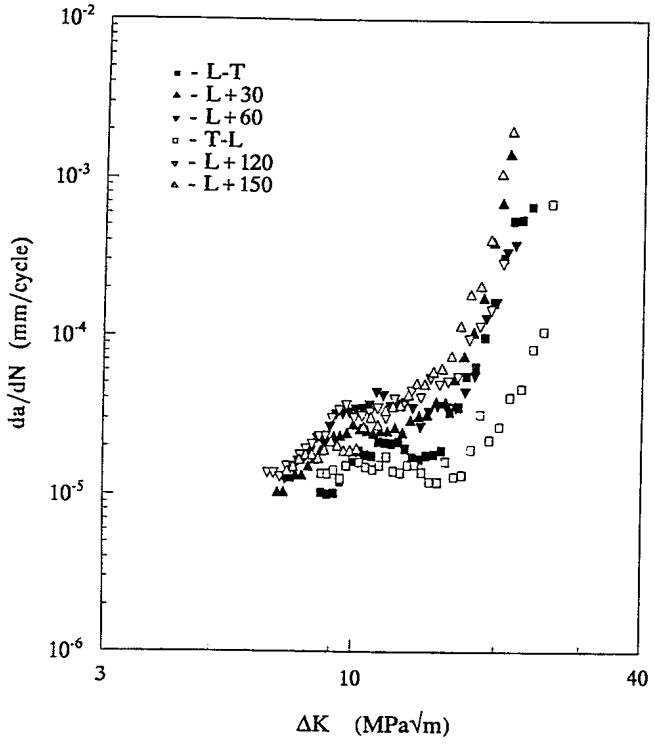

Figure 13. Fatigue crack growth rate versus stress intensity factor range for 2090-T8E41 plate at R = 0.1.

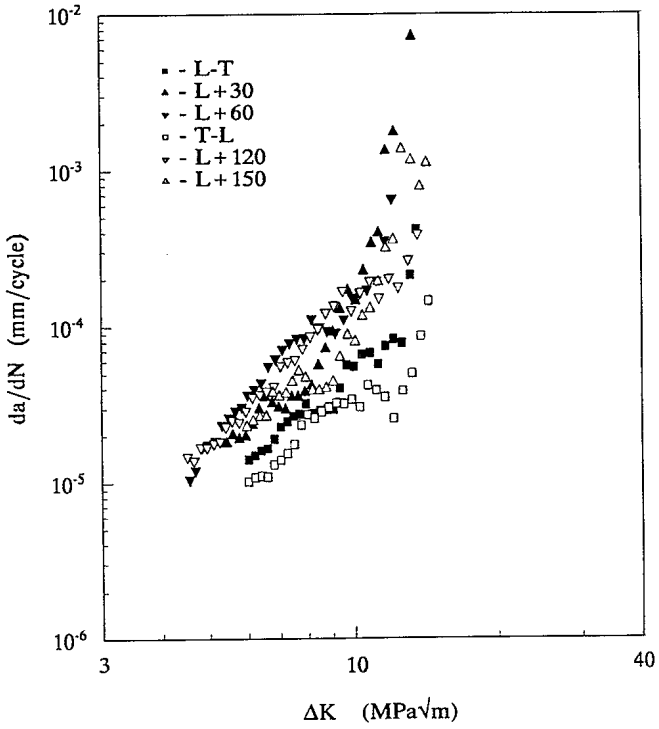

Figure 14. Crack growth rate versus stress intensity factor range for 2090 at R = 0.5.

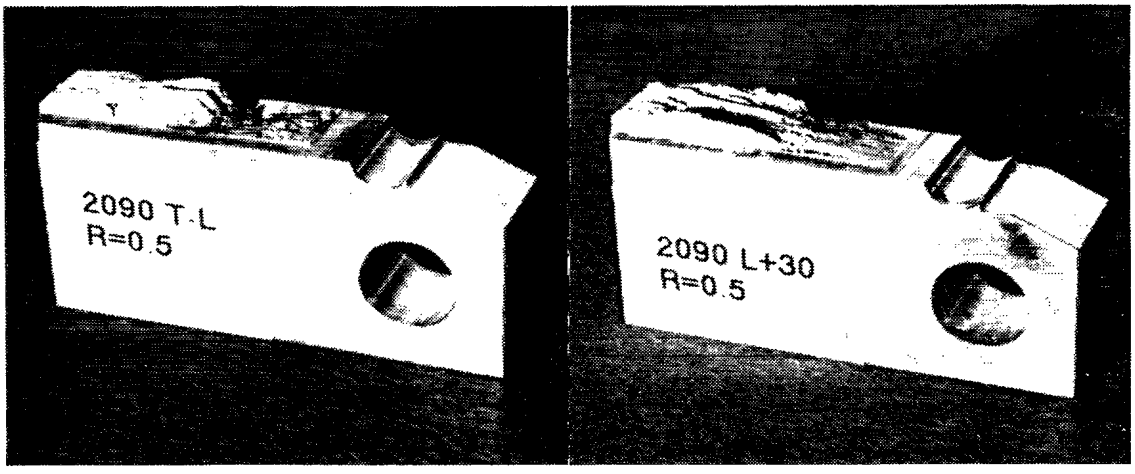

(a) (b)

Figure 15. Fracture surfaces of 2090 plate.

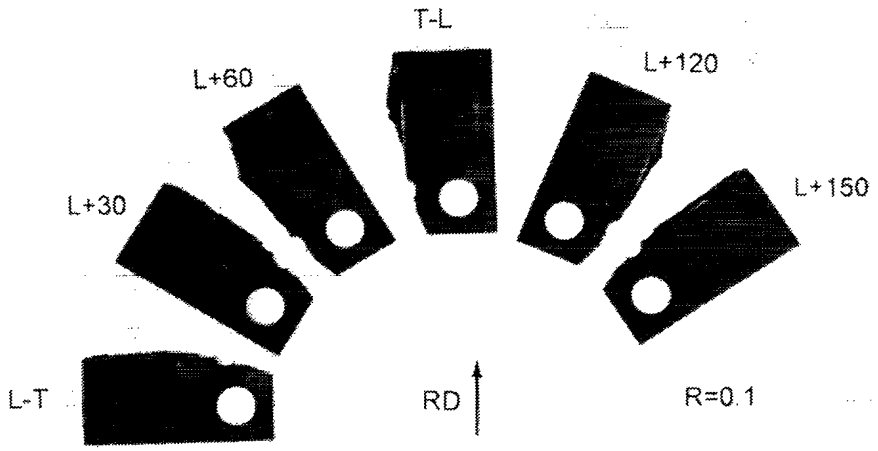

(a)

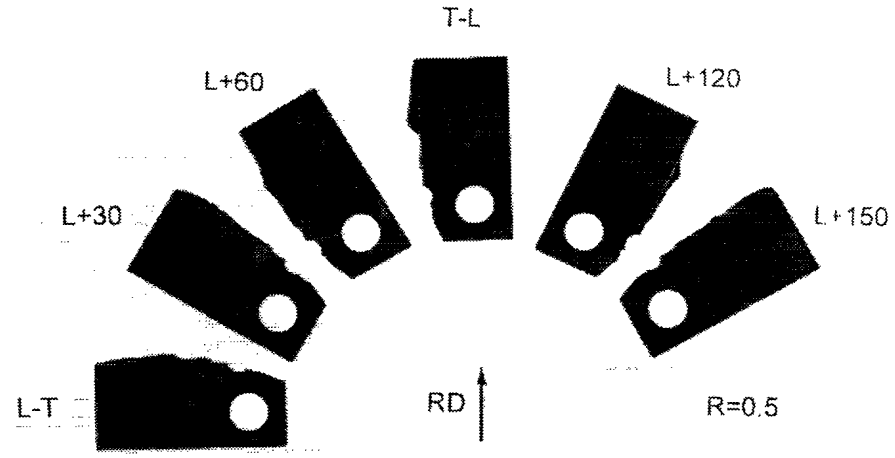

(b)

Figure 16. Profiles of broken 2090 specimens.

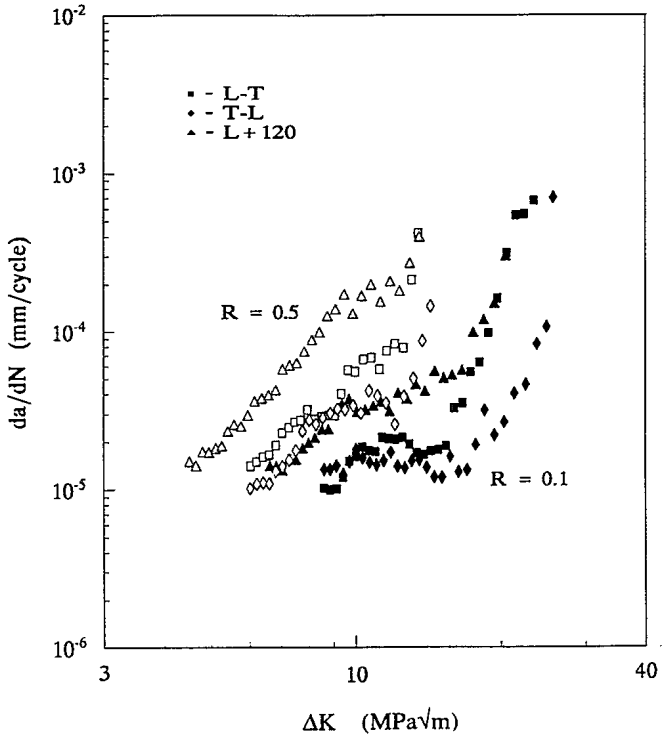

Figure 17. The effect of R ratio on crack growth in 2090. Solid symbols denote R = 0.1; open symbols R = 0.5.

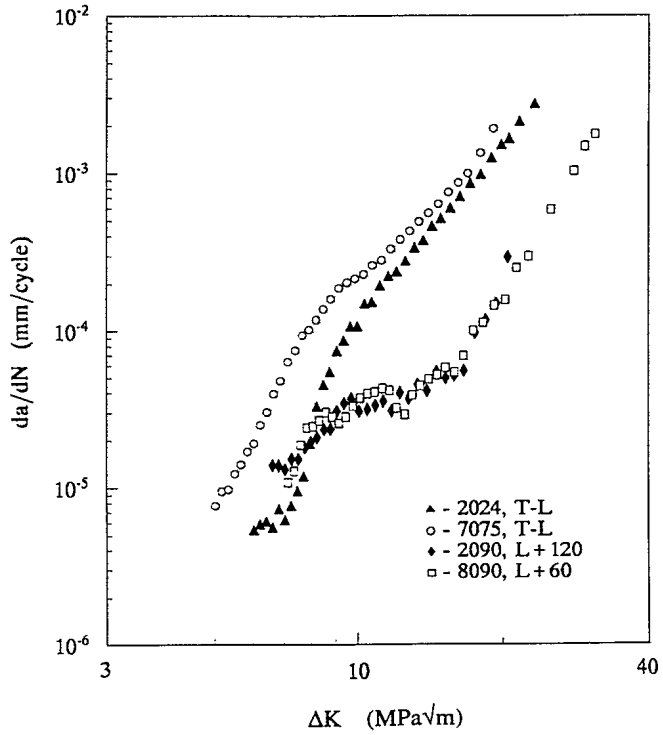

Figure 18. Comparison of crack growth rates in orientations of least resistance. R = 0.1.

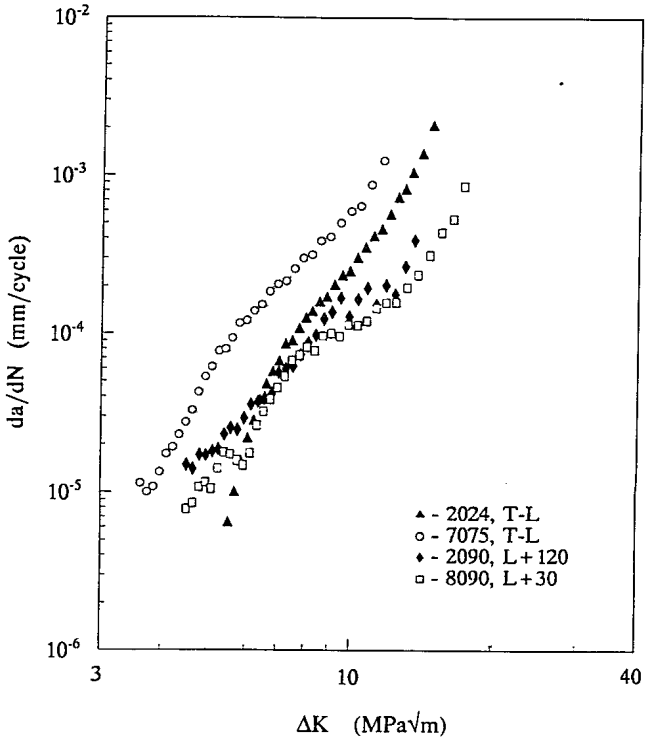

Figure 19. Comparison of crack growth rates in orientations of least resistance. R = 0.5.